

Article

TmCN@C₈₂: Monometallic Clusterfullerene Encapsulating a Tm³⁺ Ion

Huichao Zhang, Jinpeng Xin, Huaimin Jin, Wenhao Xiang, Muqing Chen , Yang-Rong Yao * and Shangfeng Yang *

Key Laboratory of Precision and Intelligent Chemistry, Department of Materials Science and Engineering, Anhui Laboratory of Advanced Photon Science and Technology, University of Science and Technology of China, Hefei 230026, China

* Correspondence: yryao@ustc.edu.cn (Y.-R.Y.); sfyang@ustc.edu.cn (S.Y.)

Abstract: Metal cyanide clusterfullerenes (CYCFs) are formed via the encapsulation of a single metal atom and a cyanide unit inside fullerene cages, endowing them with excellent properties in various applications. In this work, we report the synthesis, isolation, and characterizations of the first cases of thulium (Tm)-based CYCFs with the popular C₈₂ carbon cages. The structural elucidation of the two TmCN@C₈₂ isomers was achieved via diverse analytical techniques, including mass spectrometry, Vis-NIR spectroscopy, single-crystal X-ray crystallography, and cyclic voltammetry. The crystallographic analyses unambiguously confirmed the molecular structures of the two TmCN@C₈₂ isomers as TmCN@C_s(6)-C₈₂ and TmCN@C_{2v}(9)-C₈₂. Both TmCN clusters adopt a well-established triangular configuration, with the Tm ion located on the symmetrical plane of the carbon cages. The electronic structures of both TmCN@C₈₂ isomers adopt a Tm³⁺(CN)⁻@(C₈₂)²⁻ configuration, exhibiting characteristic spectral and electrochemical properties reminiscent of divalent endohedral metallofullerenes (EMFs). Intriguingly, unlike the divalent Tm²⁺ ion observed in the mono-metallofullerenes Tm@C_{2n}, a higher oxidation state of Tm³⁺ is identified in the monometallic TmCN cluster due to bonding with the cyanide anion. This result provides valuable insight into the essential role of the non-metallic endo-units in governing the oxidation state of the metal ion and the electronic behaviors of EMFs.

Keywords: endohedral metallofullerenes; cyanide clusterfullerenes; thulium; X-ray crystallography



Citation: Zhang, H.; Xin, J.; Jin, H.; Xiang, W.; Chen, M.; Yao, Y.-R.; Yang, S. TmCN@C₈₂: Monometallic Clusterfullerene Encapsulating a Tm³⁺ Ion. *Inorganics* **2023**, *11*, 323. <https://doi.org/10.3390/inorganics11080323>

Academic Editor: Filip Uhlík

Received: 29 June 2023

Revised: 21 July 2023

Accepted: 26 July 2023

Published: 31 July 2023



Copyright: © 2023 by the authors. Licensee MDPI, Basel, Switzerland. This article is an open access article distributed under the terms and conditions of the Creative Commons Attribution (CC BY) license (<https://creativecommons.org/licenses/by/4.0/>).

1. Introduction

Fullerene is an allotropic carbon with a great number of family members differentiated by the number of carbon atoms and structural isomerism [1]. A pristine fullerene comprises 12 pentagons and several hexagons according to the number of carbon atoms, forming a cage-like structure with a hollow cavity. Based on the unique structures of fullerenes, three strategies, including exohedral [2–4], cage skeletal [5–7], and endohedral [8–10] modifications, have been widely employed for the chemical functionalization of fullerenes. In particular, the hollow cavity can serve as a nanoscale container to encapsulate various metal atoms or metal clusters, resulting in the formation of endohedral metallofullerenes (EMFs), which have attracted significant interest due to their unique structures and excellent physical and chemical properties, which are different from those of empty fullerenes, in versatile research fields [11–13].

The exploration of EMFs began with the discovery of La@C₆₀ in 1985 [14], which sparked a surge of enthusiasm among researchers in understanding the structures, properties, and potential applications of EMFs. Over the past three decades, remarkable progress has been made, particularly with the identification of the first clusterfullerene, Sc₃N@C₈₀, in 1999, which opened doors to the encapsulation of various cluster species [15]. Subsequently, clusterfullerenes have developed dramatically as the most important branch of EMFs, with various clusters, such as metal nitride [15–17], carbide [18–21], oxide [22–25],

sulfide [26–29], and cyanide [30–39]. Among them, metal cyanide clusterfullerenes (CYCFs), which feature a distinctive mono-metallic cluster with flexible configurations, provide ideal models for regulating properties in applications such as single-molecule magnets [30,32].

To date, a wide range of CYCFs have been successfully synthesized and characterized [30–39], including MCN@C_{76} ($M = \text{Y}$ [30], Tb [30], Lu [35]) and MCN@C_{82} ($M = \text{Y}$ [31,38], Tb [32,37], Dy [33], Lu [35], U [34]), and MCN@C_{84} ($M = \text{Y}$ [36,39], Tb [36], and Dy [36]). Notably, the oxidation state of uranium in the UCN cluster remains ambiguous as it can exhibit U(I) or U(III) due to the significant donation bonding from the fullerene cage and CN^- cluster to uranium [34]. In contrast, cyanide clusters based on yttrium (Y), terbium (Tb), dysprosium (Dy), and lutetium (Lu) uniformly adopt a fixed oxidation state of +3. However, little is known about tunable lanthanide metals with variable oxidation states, such as thulium (Tm), which generally exhibit +2 or +3 oxidation states in fullerenes [40–44]. In addition, compared to the extensively studied rare earth metals, there have been limited reports on Tm-based EMFs, despite their promising applications as fluorescent probes. For example, Shinohara and co-workers demonstrated that the divalent Tm^{2+} in Tm@C_{88} isomers and trivalent Tm^{3+} in $\text{Tm}_2\text{C}_2\text{@C}_{82}$ isomers exhibit characteristic photoluminescence at 1200 and 1300–2000 nm, respectively, owing to their distinct energy level transitions [45]. Hence, it is highly desirable to explore novel Tm-based EMFs to gain insights into their bonding, structures, and applications based on their variable oxidation states.

Herein, we report the synthesis, isolation, and characterizations of the first Tm-based EMFs, $\text{TmCN@C}_{s(6)\text{-C}_{82}}$ and $\text{TmCN@C}_{2v(9)\text{-C}_{82}}$, which, to the best of our knowledge, represent the first isolated Tm-based CYCFs. These two compounds were characterized well via mass spectrometry, single-crystal X-ray diffraction, visible-near-infrared (Vis-NIR) spectroscopy, and cyclic voltammetry. The crystallographic analysis revealed a triangular configuration of the TmCN cluster within both fullerene cages. The electronic structures of both TmCN@C_{82} isomers are proposed to exhibit a $\text{Tm}^{3+}(\text{CN})^-@(\text{C}_{82})^{2-}$ configuration, displaying characteristic spectral and electrochemical properties reminiscent of divalent EMFs. Notably, a higher oxidation state of Tm^{3+} in the mono-metallic TmCN cluster, in contrast to the divalent Tm^{2+} observed in mono-metallofullerenes Tm@C_{2n} , can be attributed to the presence of the encapsulated cyanide anion.

2. Results and Discussion

Soot containing Tm-based cyanide clusterfullerenes was synthesized utilizing a modified Krätschmer–Huffman direct current (DC) arc discharge method [46]. Briefly, graphite rods were densely packed with graphite powder, Tm_2O_3 , and TiO_2 , which acts as a catalyst to enhance the yields of the Tm-based cyanide clusterfullerenes. The molar ratio of C/Tm/Ti was maintained at 15/1/1, and the arc-discharge synthesis was performed under a low-vacuum atmosphere with 200 mbar He and 10 mbar N_2 . The two targeted TmCN@C_{82} isomers were extracted from the carbon soot samples using the Soxhlet extraction method, followed by isolation via multiple-stage high-performance liquid chromatography (HPLC). The high purity of the isolated TmCN@C_{82} isomers was verified by observing a solitary peak in the HPLC chromatograms via an analytical Buckyprep column, as depicted in Figure 1. The inserted mass spectra of the two TmCN@C_{82} isomers also exhibited a solitary peak at $m/z = 1179$, further confirming their high purity. In addition, the experimental isotopic distributions of the two TmCN@C_{82} isomers show good agreement with the theoretical predictions.

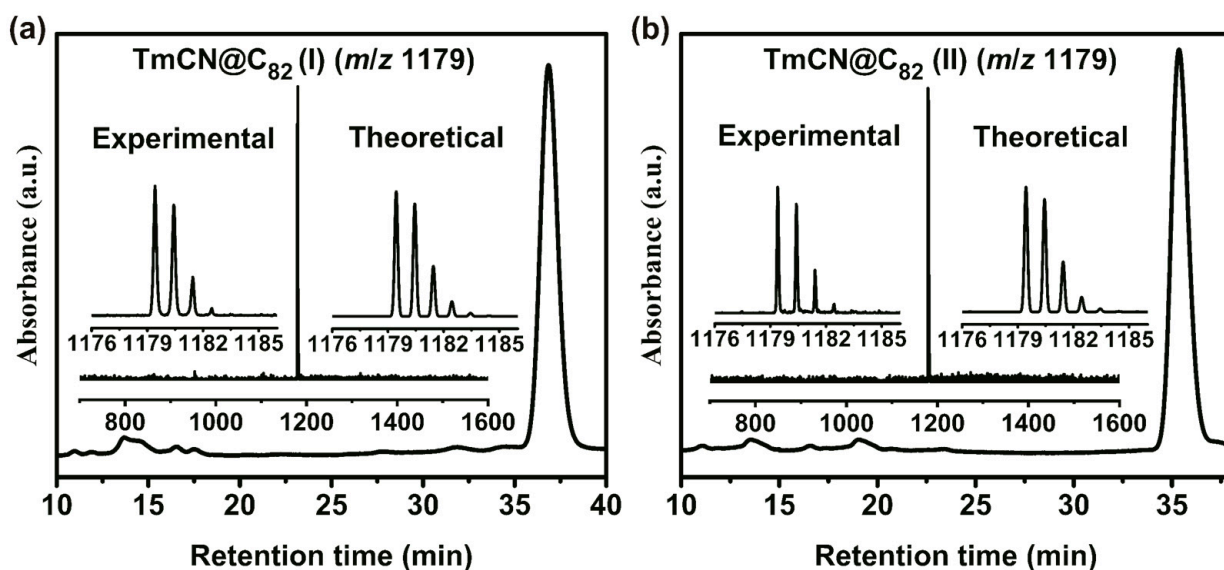


Figure 1. HPLC chromatograms of purified (a) TmCN@C₈₂ (I) and (b) TmCN@C₈₂ (II), obtained using an analytical Buckyprep column with toluene as the eluent and a flow rate of 1 mL/min. The inserts show the mass spectra of two TmCN@C₈₂ isomers with experimental versus theoretical isotopic distributions.

The molecular structures of the TmCN@C₈₂ (I) and TmCN@C₈₂ (II) were precisely characterized as TmCN@C_s(6)-C₈₂ and TmCN@C_{2v}(9)-C₈₂, respectively, via single-crystal X-ray diffraction and through their co-crystallization with decapyrrylcorannulene (DPC) molecules, which enhance the crystallinity of EMFs [47]. Both co-crystals were found to crystallize in P2₁/c, a space group of No. 14, which is commonly seen in the EMF-DPC co-crystallization systems, and the utilization of the low-symmetry primitive lattice for the EMF-DPC co-crystals could effectively circumvent the “crystallographic mirror dilemma” that generally appears in the EMF-Ni^{II}(OEP) co-crystals crystallized in the C2/m space group [48]. As shown in Figure 2a,b, the TmCN@C₈₂ isomers were co-crystallized with two DPC molecules, exhibiting a distinctive V-shaped configuration with a dihedral angle of about 65°. The closest C...C distances between both TmCN@C₈₂ isomers and the DPC molecules were measured to be ~3.37 Å; this is close to the interlayer spacing observed in graphite (3.35 Å), suggesting their π - π stacking interactions.

The encapsulated TmCN cluster, with a CN non-metallic unit supported by a mono-metallic Tm ion, adopts a triangular configuration inside both C₈₂ isomers, similar to their analogs MCN@C_s(6)-C₈₂ and MCN@C_{2v}(9)-C₈₂ (M = Y, Tb, Dy, Lu). Due to the larger electronegativity of nitrogen versus carbon, the distance of the Tm-N bond is significantly shorter than that of the Tm-C bond, and the C-N bond lengths fall in the range of typical C-N triple bonds, as shown in Figure 2c,d. The encapsulated Tm ion shows some slight disorder which is probably caused by thermal vibration. The dominant Tm site, with the most significant occupancy, is located over an s-indacene-type hexagon of the carbon cages, exhibiting Tm-cage distances in the range of 2.23–2.49 Å and 2.23–2.68 Å inside the C_s(6)-C₈₂ and C_{2v}(9)-C₈₂ carbon cages, respectively. Interestingly, the dominant Tm location is aligned with the symmetrical plane of both the C_s(6)-C₈₂ and C_{2v}(9)-C₈₂ cages, which is in perfect agreement with the recent finding of the “mirror observation” for mono-metallofullerenes, suggesting that the mono-metallic cyanide clusterfullerenes display some structural characteristics that are similar to those of mono-metallofullerenes [48].

The crystallographic results suggest the preference of the TmCN cluster for encapsulation inside the cages of C_s(6)-C₈₂ and C_{2v}(9)-C₈₂, which can be inferred from our previous work on TbCN@C₈₂ isomers [32]. TbCN@C_{2v}(9)-C₈₂ is the most stable isomer among all TbCN@C₈₂ isomers, followed by TbCN@C_s(6)-C₈₂, which is similar to the relative energy order found for the YCN@C₈₂ isomers. The results reveal that the cage cavity volumes of

$C_s(6)-C_{82}$ and $C_{2v}(9)-C_{82}$ are suitable for encapsulation of a metal cyanide cluster; this is in agreement with the theoretical studies on C_{84} isomers [49], which provided insights into the relationship between the stability of an encapsulated endo-unit and the volume of a specific carbon cage.

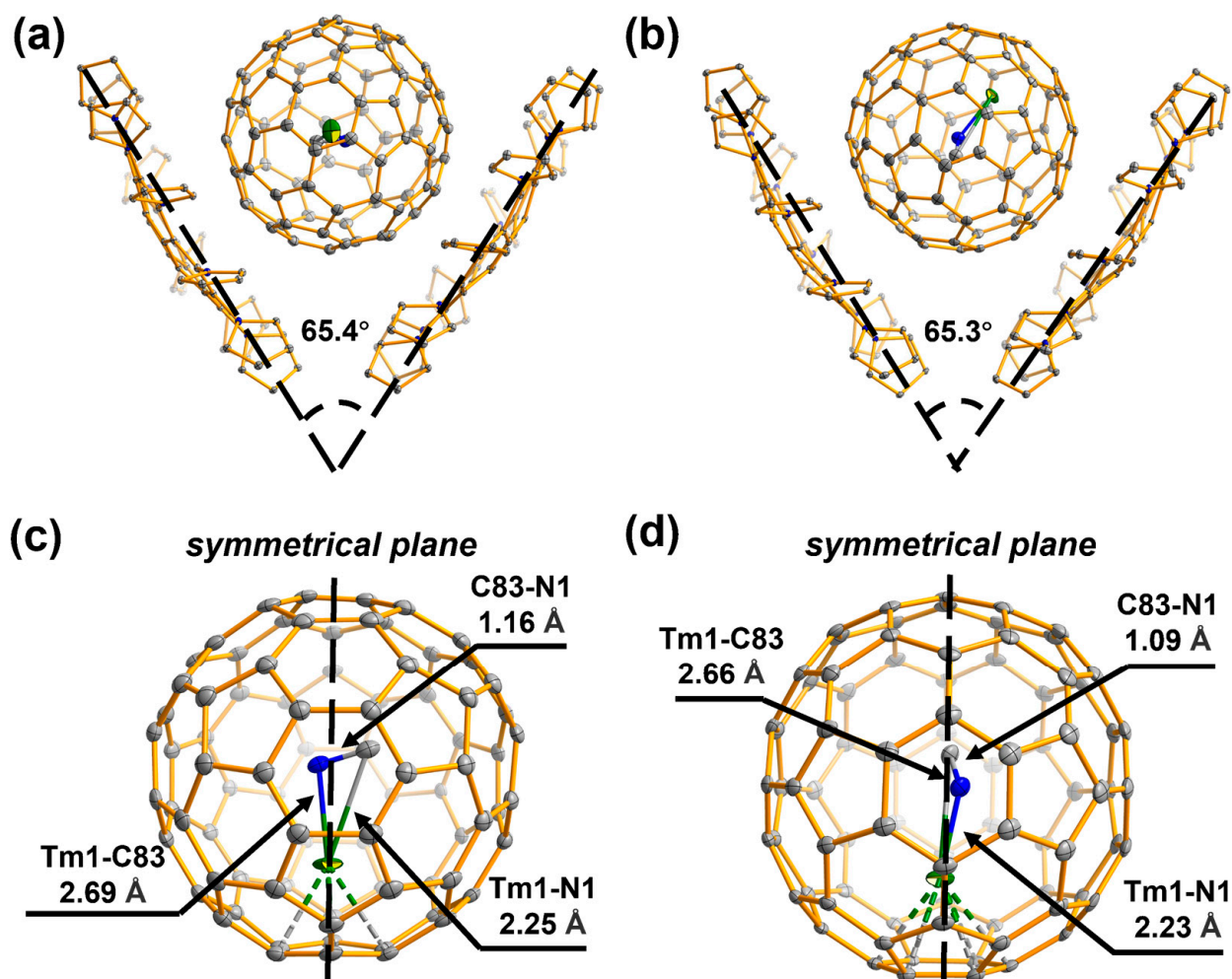


Figure 2. Oak Ridge thermal ellipsoid plot (ORTEP) drawings of crystallographic structures of the two co-crystals. (a,b) The relative orientations between two DPC molecules and (a) $TmCN@C_s(6)-C_{82}$ and (b) $TmCN@C_{2v}(9)-C_{82}$. (c,d) The relative orientations between the encapsulated $TmCN$ cluster with detailed structural information and the (c) $C_s(6)-C_{82}$ and (d) $C_{2v}(9)-C_{82}$ cages. The Tm, N, and C atoms are presented as green, blue, and gray, respectively.

The electronic properties of $TmCN@C_s(6)-C_{82}$ and $TmCN@C_{2v}(9)-C_{82}$ were investigated via visible-near infrared (Vis-NIR) spectroscopy. It is well-established that the absorption spectra of EMFs are primarily governed by the $\pi-\pi^*$ excitations of the carbon cages; thus, Vis-NIR spectroscopy is commonly employed to study the electronic structures of EMFs [12]. As shown in Figure 3, $TmCN@C_s(6)-C_{82}$ exhibits a distinct spectrum with absorptions at 510, 758, 1016, 1134, and 1334 nm, while $TmCN@C_{2v}(9)-C_{82}$ displays a strong absorption at 1338 nm, accompanied by relatively weak absorptions at 524, 622, 706, 770, 1016, and 1168 nm. The measured optical bandgap of $TmCN@C_s(6)-C_{82}$ is 0.76 V, slightly larger than that of $TmCN@C_{2v}(9)-C_{82}$ (0.71 V). The absorption features and optical bandgaps of both $TmCN@C_s(6)-C_{82}$ and $TmCN@C_{2v}(9)-C_{82}$ resemble those of Y-, Tb-, Dy-, and Lu-CYCFs (Table 1) [31–35], which share the same cage isomerism and exhibit a divalent electronic configuration. Consequently, the formal electronic configurations of the two Tm-based CYCFs can be described as $Tm^{3+}(CN)^-@C_s(6)-C_{82}^{2-}$ and $Tm^{3+}(CN)^-@C_{2v}(9)-$

C_{82}^{2-} , respectively. Notably, compared to $TmCN@C_s(6)-C_{82}$ and $TmCN@C_{2v}(9)-C_{82}$, $Tm@C_s(6)-C_{82}$ and $Tm@C_{2v}(9)-C_{82}$ display distinct absorption spectra [50–52] despite sharing the same cage isomerism. In addition, previous X-ray absorption spectroscopy (XAS) and ultraviolet photoelectron spectroscopy (UPS) studies [53,54] demonstrated that the Tm atoms prefer an oxidation state of +2 in mono-metallofullerenes. Therefore, the obtained results indicate that on one hand, the Tm ion or the TmCN cluster significantly contributes to the molecular orbitals. On the other hand, the higher oxidation state (+3) of the Tm atom in the TmCN cluster is identified due to bonding with the non-metallic CN unit.

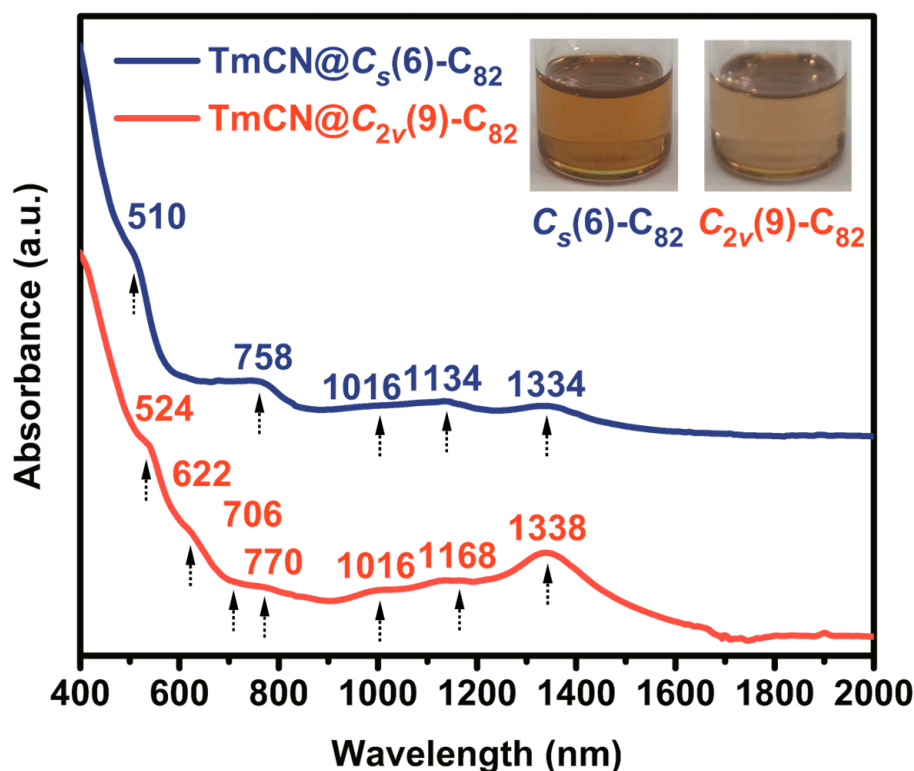


Figure 3. The Vis-NIR absorption spectra of $TmCN@C_s(6)-C_{82}$ (in blue) and $TmCN@C_{2v}(9)-C_{82}$ (in red). The inserts are photographs of the two CYCFs dissolved in CS_2 . The spectra of the two $TmCN@C_{82}$ isomers are shown together by shifting one along the ordinate axis, and the absorption peaks are indicated by black arrows.

Table 1. Vis-NIR absorption spectral data of two $TmCN@C_{82}$ isomers as well as Y-, Tb-, Dy-, and Lu-CYCFs for comparison.

Compounds	Absorption Peaks (nm)	λ_{onset} (nm)	ΔE_{gap} (eV) ¹	Note
$TmCN@C_s(6)-C_{82}$	510, 758, 1016, 1134, 1334	1624	0.76	this work
$TbCN@C_s(6)-C_{82}$	491, 744, 1072, 1132, 1318	1620	0.77	Ref [32]
$DyCN@C_s(6)-C_{82}$	497, 744, 1024, 1140, 1339	1656	0.75	Ref [33]
$LuCN@C_s(6)-C_{82}$	494, 596, 744, 1069, 1131, 1345	1638	0.76	Ref [35]
$YCN@C_s(6)-C_{82}$	491, 741, 1064, 1123, 1318	1620	0.77	Ref [31]
$TmCN@C_{2v}(9)-C_{82}$	524, 622, 706, 770, 1016, 1168, 1338	1740	0.71	This work
$TbCN@C_{2v}(9)-C_{82}$	518, 618, 710, 772, 1144, 1320	1770	0.70	Ref [32]
$DyCN@C_{2v}(9)-C_{82}$	536, 627, 1144, 1342	1785	0.69	Ref [33]
$LuCN@C_{2v}(9)-C_{82}$	512, 621, 697, 782, 1096, 1296	1680	0.74	Ref [35]

¹ $\Delta E_{gap} = 1240/\lambda_{onset}$.

Figure 4 shows the electrochemical behaviors of $\text{TmCN@C}_s(6)\text{-C}_{82}$ and $\text{TmCN@C}_{2v}(9)\text{-C}_{82}$, determined using cyclic voltammetry (CV) with tetrabutylammonium hexafluorophosphate (TBAPF_6) and ferrocene (Fc) as the supporting electrolyte and internal standard, respectively. Both show four reversible reduction steps and one reversible oxidation step, recorded as +0.55, −0.67, −0.90, −1.72, and −2.16 V for $\text{TmCN@C}_s(6)\text{-C}_{82}$ and +0.64, −0.45, −0.79, −1.60, and −1.94 for $\text{Tm@C}_{2v}(9)\text{-C}_{82}$. The full reduction potentials of $\text{TmCN@C}_s(6)\text{-C}_{82}$ are also more negatively shifted to about 0.1–0.2 V than those of $\text{Tm@C}_{2v}(9)\text{-C}_{82}$; thus, $\text{TmCN@C}_s(6)\text{-C}_{82}$ is more accessible for oxidation than $\text{Tm@C}_{2v}(9)\text{-C}_{82}$. Notably, the electrochemical gap of $\text{TmCN@C}_s(6)\text{-C}_{82}$ (1.22 V) is larger than that of $\text{Tm@C}_{2v}(9)\text{-C}_{82}$ (1.09 V), which results from the relatively more significant difference in their first reduction potentials.

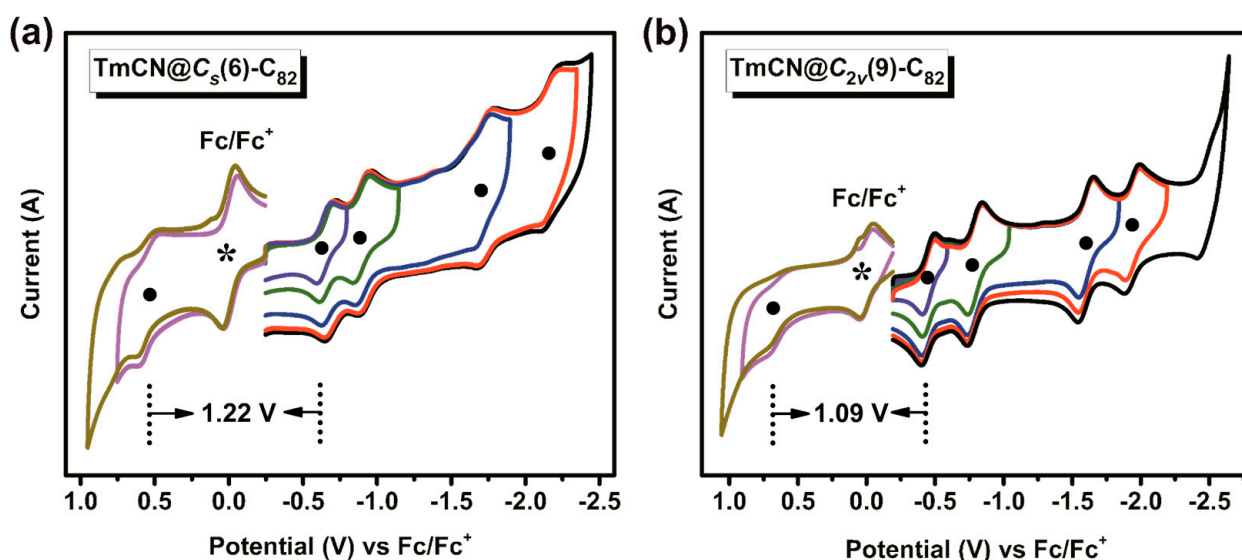


Figure 4. Cyclic voltammograms of (a) $\text{TmCN@C}_s(6)\text{-C}_{82}$ and (b) $\text{TmCN@C}_{2v}(9)\text{-C}_{82}$ in a *o*-DCB solution with a scan rate of $100 \text{ mV}\cdot\text{s}^{-1}$. TBAPF_6 and Fc were employed as the internal standard and supporting electrolyte, respectively. Black circles and asterisks are presented to show the redox and the Fc/Fc^+ peaks.

The comparison of the two TmCN@C_{82} isomers and other mono-metallic EMFs based on $\text{C}_s(6)\text{-C}_{82}$ and $\text{C}_{2v}(9)\text{-C}_{82}$ was also studied, as shown in Table 2. The redox behaviors of $\text{TmCN@C}_s(6)\text{-C}_{82}$ and $\text{TmCN@C}_{2v}(9)\text{-C}_{82}$ are fairly similar to those of the corresponding Y-, Tb-, Dy-, and Lu-CYCF counterparts [31–35], suggesting that both TmCN@C_{82} isomers bear a divalent electronic configuration of $\text{Tm}^{3+}(\text{CN})^-\text{@}(\text{C}_s(6)\text{-C}_{82})^{2-}$, which is in agreement with the spectroscopic result. Similar redox behaviors between divalent M@C_{82} isomers, such as $\text{Yb@C}_s(6)\text{-C}_{82}$ and $\text{Yb@C}_{2v}(9)\text{-C}_{82}$ [55] and TmCN@C_{82} isomers further confirm the electronic configurations of $\text{Tm}^{3+}(\text{CN})^-\text{@}(\text{C}_{82})^{2-}$ for both $\text{C}_s(6)$ and $\text{C}_{2v}(9)$ isomerisms. In comparison, trivalent mono-metallofullerenes ($\text{M}^{3+}\text{@}(\text{C}_{82})^{3-}$ ($\text{M} = \text{Y}$ [56], La [57,58], Pr [59], Er [60], and U [61], etc.) based on $\text{C}_s(6)$ and $\text{C}_{2v}(9)$ cage isomerism exhibit sharply different redox potentials with much more negatively shifted first oxidation potentials and much smaller electrochemical gaps. These phenomena originate from the three-electron charge transfer of $(\text{M}^{3+})\text{@}(\text{C}_{82})^{3-}$, which results in an open-shell electronic structure, while $\text{TmCN@C}_s(6)\text{-C}_{82}$ and $\text{TmCN@C}_{2v}(9)\text{-C}_{82}$ have a closed-shell electronic structures due to the two-electron transfer from the encapsulated TmCN cluster to the carbon cages.

Table 2. Redox potentials (V *vs.* Fc/Fc⁺) and electrochemical gaps of TmCN@C_s(6)-C₈₂ and TmCN@C_{2v}(9)-C₈₂ and the corresponding cyanide metallofullerenes MCN@C₈₂ and mono-metallofullerene M@C₈₂ isomers.

Compounds	^{ox} E ₁	^{red} E ₁	^{red} E ₂	^{red} E ₃	^{red} E ₄	ΔE _{gap} (eV)	Note
TmCN@C _s (6)-C ₈₂	0.55	−0.67	−0.90	−1.72	−2.16	1.22	This work
TbCN@C _s (6)-C ₈₂	0.55	−0.59	−0.84	−1.77	−1.92	1.14	Ref [32]
DyCN@C _s (6)-C ₈₂	0.56	−0.58	−0.84	1.77	−1.92	1.14	Ref [33]
LuCN@C _s (6)-C ₈₂	0.52	−0.58	−0.90	−1.69	−1.86	1.10	Ref [35]
YCN@C _s (6)-C ₈₂	0.56	−0.59	−0.84	−1.76	−1.92	1.15	Ref [31]
La@C _s (6)-C ₈₂	−0.07	−0.47	−1.40	−2.01	−2.40	0.40	Ref [57]
Pr@C _s (6)-C ₈₂	−0.07	−0.48	−1.39	−1.99	/	0.41	Ref [59]
Er@C _s (6)-C ₈₂	−0.09	−0.44	−1.46	−2.04	−2.46	0.35	Ref [60]
Y@C _s (6)-C ₈₂	−0.07	−0.43	−1.43	−2.05	/	0.36	Ref [56]
Yb@C _s (6)-C ₈₂	0.34	−0.62	−0.92	−1.81	−2.01	0.94	Ref [55]
TmCN@C _{2v} (9)-C ₈₂	0.64	−0.45	−0.79	−1.60	−1.94	1.09	This work
TbCN@C _{2v} (9)-C ₈₂	0.55	−0.46	−0.81	−1.78	−1.96	1.01	Ref [32]
DyCN@C _{2v} (9)-C ₈₂	0.56	−0.45	−0.81	−1.78	−1.96	1.01	Ref [33]
LuCN@C _{2v} (9)-C ₈₂	0.50	−0.54	−0.96	−1.71	−1.93	1.04	Ref [35]
La@C _{2v} (9)-C ₈₂	0.07	−0.42	−1.37	−1.53	−2.26	0.49	Ref [58]
Pr@C _{2v} (9)-C ₈₂	0.07	−0.39	−1.35	−1.46	−2.21	0.46	Ref [59]
Er@C _{2v} (9)-C ₈₂	0.08	−0.42	−1.40	−2.18	/	0.50	Ref [60]
U@C _{2v} (9)-C ₈₂	0.10	−0.43	−1.42	−1.76	−1.77	0.53	Ref [61]
Y@C _{2v} (9)-C ₈₂	0.10	−0.34	−1.34	−2.22	/	0.44	Ref [56]
Yb@C _{2v} (9)-C ₈₂	0.61	−0.46	−0.78	−1.60	−1.90	1.07	Ref [55]

3. Materials and Methods

Materials. The reagents used in this work were Tm₂O₃ (99.99%, Suzhou Rare Earth New Materials Co., Suzhou, China), TiO₂ (99%, Sinopharm Chemical Reagent Co., Ltd., Ningbo, China), CS₂ (99%, Sinopharm Chemical Reagent Co., Ltd.), toluene (99%, Sinopharm Chemical Reagent Co., Ltd.), tetrabutylammonium hexafluorophosphate (electrochemical-grade, Shanghai Aladdin Biochemical Technology Co., Ltd., Shanghai, China), 1,2-dichlorobenzene (99%, Shanghai Aladdin Biochemical Technology Co., Ltd.), and graphite rods and graphite powder (Sinosteel Shanghai New Graphite Material Co., Shanghai, China).

Synthesis of TmCN@C₈₂ isomers. Soot containing TmCN@C₈₂ isomers was synthesized using a modified Krätschmer–Huffman DC arc discharge method. Graphite rods packed with graphite powder, Tm₂O₃, and TiO₂, with a C/Tm/Ti molar ratio of 15/1/1, were preheated in a tube furnace at 1000 °C for 20 h under a nitrogen atmosphere. Subsequently, the preheated graphite rods were installed in a VDK-250 arc discharge reactor (Beijing Technol Science Co., Ltd., Beijing, China) under a low-vacuum atmosphere with 200 mbar He and 10 mbar N₂, followed by vaporization in a DC of 120 A. The two TmCN@C₈₂ isomers were extracted from the carbon soot with CS₂ using the Soxhlet extraction method. The resulting fullerene solution in CS₂ was evaporated and then dissolved again in toluene, followed by concentration for the following multi-stage HPLC procedures [62,63].

Isolation of TmCN@C₈₂ isomers. As illustrated in Figure 5, a four-stage HPLC process was employed to purify the two TmCN@C₈₂ isomers, and toluene was employed as the eluent in all stages. The first stage was performed on a preparative 5PYE column (20 × 250 mm) with a 15 mL/min flow rate, and fraction A, which contained the two TmCN@C₈₂ isomers and other fullerenes, was collected, concentrated, and then re-injected into the HPLC. In the second stage, a recycling mode was employed on a preparative Buckyprep-M column (20 × 250 mm) with a 12 mL/min flow rate. After three runs of recycling, fraction A-4, which contained the TmCN@C₈₂ isomers, was collected for the next stage. A semi-preparative 5PBB column (10 × 250 mm, 4 mL/min flow rate) was used in the third separation stage to remove the other mixed fullerenes in the A-4 fraction. Fraction A-4-3 was found to contain only two TmCN@C₈₂ isomers, and all the impurity fullerenes had been removed. In the last stage, a recycling HPLC process was employed to purify the two isomers, using a semi-preparative Buckyprep column (10 × 250 mm) with a 4 mL/min flow rate. After 13 recycling runs, purified TmCN@C_s(6)-C₈₂, labeled as

A-4-3-1, and TmCN@C_{2v}(9)-C₈₂, labeled as A-4-3-2, were individually collected for further characterizations. The detailed fraction information for each stage is shown in Table 3.

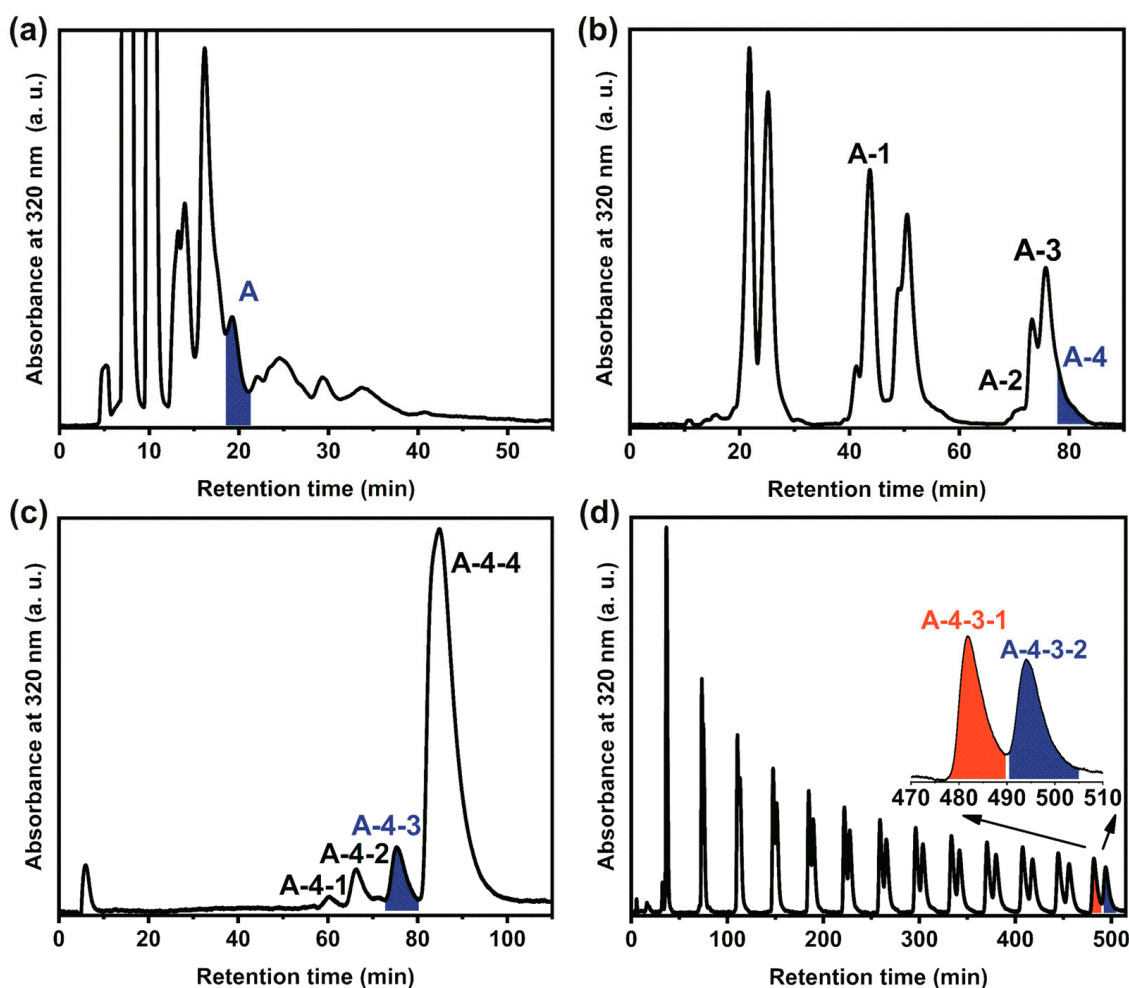


Figure 5. HPLC isolation procedure for TmCN@C_s(6)-C₈₂ and TmCN@C_{2v}(9)-C₈₂. (a) the first stage of HPLC isolation procedure on a preparative 5PYE column (20 × 250 mm). (b) the second stage of HPLC isolation procedure on a preparative Buckyprep-M column (20 × 250 mm). (c) the third stage of HPLC isolation procedure on a semi-preparative 5PBB column (10 × 250 mm). (d) the fourth stage of HPLC isolation procedure on a semi-preparative Buckyprep column (10 × 250 mm). The insert in (d) shows the recycled fractions of A-4-3-1 (red) and A-4-3-2 (blue), which represent the purified TmCN@C_s(6)-C₈₂ and TmCN@C_{2v}(9)-C₈₂, respectively.

Table 3. The major eluted components in each HPLC fraction and their relative abundances.

Fraction	Subfraction	Major Component	Relative Abundance
A	A-1	C ₈₄₋₈₆	46.1%
	A-2	Tm@C ₈₂ /TmC ₇₇ N	3.4%
	A-3	Tm@C ₈₀₋₈₄ /TmC ₈₃ N	36.7%
	A-4	Tm@C _{80,84} /Ti ₂ C ₈₀ /TmCN@C ₈₂	13.8%
A-4	A-4-1	Ti ₂ C ₈₀	2.2%
	A-4-2	Tm@C ₈₀	6.5%
	A-4-3	TmCN@C ₈₂ (C _s (6), C _{2v} (9))	8.7%
	A-4-4	Tm@C ₈₄	82.6%
A-4-3	A-4-3-1	TmCN@C _s (6)-C ₈₂	52.1%
	A-4-3-2	TmCN@C _{2v} (9)-C ₈₂	47.9%

Spectroscopic studies. The mass spectra of the two TmCN@C₈₂ isomers were recorded on an Autoflex III matrix-assisted laser desorption ionization time-of-flight mass spectrometer (MALDI-TOF-MS, Bruker, Germany) under positive mode. The Vis-NIR spectra of the purified samples were measured using a UV-3600 spectrometer (Shimadzu, Japan).

Electrochemical analysis. The electrochemical study was performed in a CHI 660 potentiostat (CH Instrument, USA) using a three-electrode system, including a glassy carbon working electrode, a platinum (Pt) wire counter electrode, and a silver (Ag) wire reference electrode. Tetrabutylammonium hexafluorophosphate (TBAPF₆) and ferrocene (Fc) were employed as the supporting electrolyte and the internal standard, respectively. TBAPF₆, Fc, and the samples were all dissolved in 1,2-dichlorobenzene (*o*-DCB).

X-ray crystallographic study. The co-crystals of the DPC molecules and EMF samples were obtained by slowly laying a DPC toluene solution onto an EMF CS₂ solution in a nuclear magnetic resonance (NMR) tube. Black block co-crystals of a suitable size for X-ray diffraction analysis were observed on the wall or in the bottom after 10–15 days. The crystallographic data were collected in the BL17B beamline station at Shanghai Synchrotron Radiation Facility. The crystallographic structures were solved using SHELXT-2014 via the intrinsic phasing method and then refined with SHELXL-2018 via the full-matrix least-squares method based on F^2 within the software Olex2 [64,65]. The SQUEEZE program [66] included in the PLATON program was employed to calculate the contribution of the disordered toluene solvents. The detailed crystallographic data of the two co-crystals are shown in Table 4.

Table 4. Crystallographic information of two TmCN@C₈₂ co-crystals.

Crystal	TmCN@C _s (6)-C ₈₂	TmCN@C _{2v} (9)-C ₈₂
Empirical formula	C ₂₁₀ H ₈₈ N ₂₁ Tm	C ₂₁₀ H ₈₈ N ₂₁ Tm
Formula weight	3073.94	3073.94
Habit	Block	Block
Temperature, K	100	100
Crystal system	Monoclinic	Monoclinic
Space group	$P2_1/c$	$P2_1/c$
<i>a</i> , Å	14.669	14.724
<i>b</i> , Å	32.146	32.032
<i>c</i> , Å	32.213	32.215
α , deg	90	90
β , deg	101.74	101.91
γ , deg	90	90
Volume, Å ³	14,872.3	14,866.8
<i>Z</i>	4	4
<i>D_x</i> , g/cm ³	1.373	1.373
<i>F</i> (000)	6256	6256
Crystal Size, mm ³	0.06 × 0.03 × 0.01	0.12 × 0.08 × 0.03
2 θ max, °	20.499	24.712
R_1/wR_2 ($I > 2\sigma(I)$) ¹	0.1193/0.2831	0.0937/0.2531
GOF	1.116	1.052
Completeness	0.972	0.987
Obs reflects	5752	14,863
Total reflects	14,478	25,026
Parameters	2131	2162
metal disorder	Tm1(0.60)/Tm2(0.08)/Tm3(0.17)/ Tm4(0.11)/Tm5(0.04)	Tm1(0.25)/Tm2(0.14)/Tm3(0.09)/Tm4(0.04)/ Tm5(0.08)/Tm6(0.13)/ Tm7(0.20)/Tm8(0.07)

$$^1R_1 = \sum ||F_o| - |F_c|| / \sum |F_o|, wR_2 = [\sum w(F_o^2 - F_c^2)^2] / \sum w(F_o^2)^2]^{1/2}$$

4. Conclusions

In conclusion, we report the synthesis, isolation, and characterization of the first Tm-based CYCFs with the popular C₈₂ carbon cages via mass spectrometry, single-crystal X-ray crystallography, UV-vis-NIR spectroscopy, and cyclic voltammetry. The molecular structures of these two TmCN@C₈₂ were unambiguously determined to be TmCN@C_s(6)-C₈₂ and TmCN@C_{2v}(9)-C₈₂. The TmCN cluster bears a popular triangular configuration, and the Tm ion is located in one symmetrical plane of the carbon cage for both C_s(6)-C₈₂ and C_{2v}(9)-C₈₂. In addition, the two TmCN@C₈₂ isomers feature the characteristic spectral and electrochemical properties of divalent EMFs, suggesting a closed-shell electronic structure described as Tm³⁺(CN)⁻@(C₈₂)²⁻. Compared to the Tm@C₈₂ isomers, which contain a divalent Tm²⁺ ion, the 3+ oxidation state of the Tm atom in the mono-metallic TmCN cluster is identified due to bonding with the encapsulated cyanide anion.

Author Contributions: Conceptualization, S.Y.; funding acquisition, Y.-R.Y. and S.Y.; investigation, H.Z., J.X., H.J., and W.X.; project administration, S.Y.; supervision, Y.-R.Y. and S.Y.; writing—original draft, H.Z. and Y.-R.Y.; writing—review and editing, M.C., Y.-R.Y. and S.Y. All authors have read and agreed to the published version of the manuscript.

Funding: This research was funded by the National Natural Science Foundation of China (51925206 and U1932214) and the Fundamental Research Funds for the Central Universities (WK2060000051).

Data Availability Statement: The crystallographic data can be obtained free of charge from the Cambridge Crystallographic Data Centre with the CCDC numbers 2253745 and 2253746 via www.ccdc.cam.ac.uk/data_request/cif (accessed on 31 August 2022). The other data are available upon reasonable request from the corresponding authors.

Acknowledgments: We thank the staff in the BL17B beamline of the National Facility for Protein Science Shanghai (NFPS) at the Shanghai Synchrotron Radiation Facility for their assistance during the crystallographic data collection.

Conflicts of Interest: The authors declare no conflict of interest.

References

1. Kroto, H.W.; Heath, J.R.; O'Brien, S.C.; Curl, R.F.; Smalley, R.E. C₆₀: Buckminsterfullerene. *Nature* **1985**, *318*, 162–163. [[CrossRef](#)]
2. Xie, S.-Y.; Gao, F.; Lu, X.; Huang, R.-B.; Wang, C.-R.; Zhang, X.; Liu, M.-L.; Deng, S.-L.; Zheng, L.-S. Capturing the Labile Fullerene[50] as C₅₀Cl₁₀. *Science* **2004**, *304*, 699. [[CrossRef](#)] [[PubMed](#)]
3. Tan, Y.-Z.; Xie, S.-Y.; Huang, R.-B.; Zheng, L.-S. The stabilization of fused-pentagon fullerene molecules. *Nat. Chem.* **2009**, *1*, 450–460. [[CrossRef](#)] [[PubMed](#)]
4. Tian, H.-R.; Chen, M.-M.; Wang, K.; Chen, Z.-C.; Fu, C.-Y.; Zhang, Q.; Li, S.-H.; Deng, S.-L.; Yao, Y.-R.; Xie, S.-Y.; et al. An Unconventional Hydrofullerene C₆₆H₄ with Symmetric Heptagons Retrieved in Low-Pressure Combustion. *J. Am. Chem. Soc.* **2019**, *141*, 6651–6657. [[CrossRef](#)]
5. Su, Y.; Chen, Z.-C.; Tian, H.-R.; Xu, Y.-Y.; Zhang, Q.; Xie, S.-Y.; Zheng, L.-S. Implications of Nitrogen Doping on Geometrical and Electronic Structure of the Fullerene Dimers. *Chin. J. Chem.* **2021**, *39*, 93–98. [[CrossRef](#)]
6. Xiang, W.; Jiang, X.; Yao, Y.-R.; Xin, J.; Jin, H.; Guan, R.; Zhang, Q.; Chen, M.; Xie, S.-Y.; Popov, A.A.; et al. Monometallic Endohedral Azafullerene. *J. Am. Chem. Soc.* **2022**, *144*, 21587–21595. [[CrossRef](#)]
7. Hu, Z.; Dong, B.-W.; Liu, Z.; Liu, J.-J.; Su, J.; Yu, C.; Xiong, J.; Shi, D.-E.; Wang, Y.; Wang, B.-W.; et al. Endohedral Metallofullerene as Molecular High Spin Qubit: Diverse Rabi Cycles in Gd₂@C₇₉N. *J. Am. Chem. Soc.* **2018**, *140*, 1123–1130. [[CrossRef](#)]
8. Yao, Y.-R.; Chen, Z.-C.; Chen, L.; Zheng, S.-Y.; Yang, S.; Deng, S.-L.; Echegoyen, L.; Tan, Y.-Z.; Xie, S.-Y.; Zheng, L.-S. Two Metastable Endohedral Metallofullerenes Sc₂C₂@C₁(39656)-C₈₂ and Sc₂C₂@C₁(51383)-C₈₄: Direct-C₂-Insertion Products from Their Most Stable Precursors. *J. Am. Chem. Soc.* **2023**. [[CrossRef](#)]
9. Yao, Y.-R.; Shi, X.-M.; Zheng, S.-Y.; Chen, Z.-C.; Xie, S.-Y.; Huang, R.-B.; Zheng, L.-S. Atomically Precise Insights into Metal-Metal Bonds Using Comparable Endo-Units of Sc₂ and Sc₂C₂. *CCS Chem.* **2021**, *3*, 294–302. [[CrossRef](#)]
10. Jiang, H.; Yu, X.; Guo, M.; Yao, Y.-R.; Meng, Q.; Echegoyen, L.; Autschbach, J.; Chen, N. USc₂C₂ and USc₂NC Clusters with U-C Triple Bond Character Stabilized Inside Fullerene Cages. *J. Am. Chem. Soc.* **2023**, *145*, 5645–5654. [[CrossRef](#)]
11. Rodríguez-Forteza, A.; Balch, A.L.; Poblet, J.M. Endohedral metallofullerenes: A unique host–guest association. *Chem. Soc. Rev.* **2011**, *40*, 3551–3563. [[CrossRef](#)] [[PubMed](#)]
12. Popov, A.A.; Yang, S.; Dunsch, L. Endohedral Fullerenes. *Chem. Rev.* **2013**, *113*, 5989–6113. [[CrossRef](#)] [[PubMed](#)]
13. Yang, S.; Wei, T.; Jin, F. When metal clusters meet carbon cages: Endohedral clusterfullerenes. *Chem. Soc. Rev.* **2017**, *46*, 5005–5058. [[CrossRef](#)] [[PubMed](#)]

14. Heath, J.R.; O'Brien, S.C.; Zhang, Q.; Liu, Y.; Curl, R.F.; Tittel, F.K.; Smalley, R.E. Lanthanum complexes of spheroidal carbon shells. *J. Am. Chem. Soc.* **1985**, *107*, 7779–7780. [[CrossRef](#)]
15. Stevenson, S.; Rice, G.; Glass, T.; Harich, K.; Cromer, F.; Jordan, M.R.; Craft, J.; Hadju, E.; Bible, R.; Olmstead, M.M.; et al. Small-bandgap endohedral metallofullerenes in high yield and purity. *Nature* **1999**, *401*, 55–57. [[CrossRef](#)]
16. Li, X.; Roselló, Y.; Yao, Y.-R.; Zhuang, J.; Zhang, X.; Rodríguez-Fortea, A.; de Graaf, C.; Echegoyen, L.; Poblet, J.M.; Chen, N. $U_2N@I_h(7)-C_{80}$: Fullerene cage encapsulating an unsymmetrical U(IV)=N=U(V) cluster. *Chem. Sci.* **2021**, *12*, 282–292. [[CrossRef](#)]
17. Meng, Q.; Abella, L.; Yao, Y.-R.; Sergentu, D.-C.; Yang, W.; Liu, X.; Zhuang, J.; Echegoyen, L.; Autschbach, J.; Chen, N. A charged diatomic triple-bonded $U\equiv N$ species trapped in C_{82} fullerene cages. *Nat. Commun.* **2022**, *13*, 7192. [[CrossRef](#)]
18. Wang, C.-R.; Kai, T.; Tomiyama, T.; Yoshida, T.; Kobayashi, Y.; Nishibori, E.; Takata, M.; Sakata, M.; Shinohara, H. A Scandium Carbide Endohedral Metallofullerene: $(Sc_2C_2)@C_{84}$. *Angew. Chem. Int. Ed.* **2001**, *40*, 397–399. [[CrossRef](#)]
19. Wang, T.-S.; Chen, N.; Xiang, J.-F.; Li, B.; Wu, J.-Y.; Xu, W.; Jiang, L.; Tan, K.; Shu, C.-Y.; Lu, X.; et al. Russian-Doll-Type Metal Carbide Endofullerene: Synthesis, Isolation, and Characterization of $Sc_4C_2@C_{80}$. *J. Am. Chem. Soc.* **2009**, *131*, 16646–16647. [[CrossRef](#)]
20. Zhang, X.; Li, W.; Feng, L.; Chen, X.; Hansen, A.; Grimme, S.; Fortier, S.; Sergentu, D.-C.; Duignan, T.J.; Autschbach, J.; et al. A diuranium carbide cluster stabilized inside a C_{80} fullerene cage. *Nat. Commun.* **2018**, *9*, 2753. [[CrossRef](#)]
21. Zhuang, J.; Abella, L.; Sergentu, D.-C.; Yao, Y.-R.; Jin, M.; Yang, W.; Zhang, X.; Li, X.; Zhang, D.; Zhao, Y.; et al. Diuranium(IV) Carbide Cluster U_2C_2 Stabilized Inside Fullerene Cages. *J. Am. Chem. Soc.* **2019**, *141*, 20249–20260. [[CrossRef](#)] [[PubMed](#)]
22. Stevenson, S.; Mackey, M.A.; Stuart, M.A.; Phillips, J.P.; Easterling, M.L.; Chancellor, C.J.; Olmstead, M.M.; Balch, A.L. A Distorted Tetrahedral Metal Oxide Cluster inside an Icosahedral Carbon Cage. Synthesis, Isolation, and Structural Characterization of $Sc_4(\mu_3-O)_2@I_h-C_{80}$. *J. Am. Chem. Soc.* **2008**, *130*, 11844–11845. [[CrossRef](#)] [[PubMed](#)]
23. Mercado, B.Q.; Olmstead, M.M.; Beavers, C.M.; Easterling, M.L.; Stevenson, S.; Mackey, M.A.; Coumbe, C.E.; Phillips, J.D.; Phillips, J.P.; Poblet, J.M.; et al. A seven atom cluster in a carbon cage, the crystallographically determined structure of $Sc_4(\mu_3-O)_3@I_h-C_{80}$. *Chem. Commun.* **2010**, *46*, 279–281. [[CrossRef](#)] [[PubMed](#)]
24. Velkos, G.; Yang, W.; Yao, Y.-R.; Sudarkova, S.M.; Liu, X.; Büchner, B.; Avdoshenko, S.M.; Chen, N.; Popov, A.A. Shape-adaptive single-molecule magnetism and hysteresis up to 14 K in oxide clusterfullerenes $Dy_2O@C_{72}$ and $Dy_2O@C_{74}$ with fused pentagon pairs and flexible Dy–(μ_2-O)–Dy angle. *Chem. Sci.* **2020**, *11*, 4766–4772. [[CrossRef](#)]
25. Mercado, B.Q.; Stuart, M.A.; Mackey, M.A.; Pickens, J.E.; Confait, B.S.; Stevenson, S.; Easterling, M.L.; Valencia, R.; Rodríguez-Fortea, A.; Poblet, J.M.; et al. $Sc_2(\mu_2-O)$ Trapped in a Fullerene Cage: The Isolation and Structural Characterization of $Sc_2(\mu_2-O)@C_5(6)-C_{82}$ and the Relevance of the Thermal and Entropic Effects in Fullerene Isomer Selection. *J. Am. Chem. Soc.* **2010**, *132*, 12098–12105. [[CrossRef](#)]
26. Dunsch, L.; Yang, S.; Zhang, L.; Svitova, A.; Oswald, S.; Popov, A.A. Metal Sulfide in a C_{82} Fullerene Cage: A New Form of Endohedral Clusterfullerenes. *J. Am. Chem. Soc.* **2010**, *132*, 5413–5421. [[CrossRef](#)]
27. Chen, N.; Beavers, C.M.; Mulet-Gas, M.; Rodríguez-Fortea, A.; Munoz, E.J.; Li, Y.-Y.; Olmstead, M.M.; Balch, A.L.; Poblet, J.M.; Echegoyen, L. $Sc_2S@C_5(10528)-C_{72}$: A Dimetallic Sulfide Endohedral Fullerene with a Non Isolated Pentagon Rule Cage. *J. Am. Chem. Soc.* **2012**, *134*, 7851–7860. [[CrossRef](#)]
28. Chen, N.; Mulet-Gas, M.; Li, Y.-Y.; Stene, R.E.; Atherton, C.W.; Rodríguez-Fortea, A.; Poblet, J.M.; Echegoyen, L. $Sc_2S@C_2(7892)-C_{70}$: A metallic sulfide cluster inside a non-IPR C_{70} cage. *Chem. Sci.* **2013**, *4*, 180–186. [[CrossRef](#)]
29. Mercado, B.Q.; Chen, N.; Rodríguez-Fortea, A.; Mackey, M.A.; Stevenson, S.; Echegoyen, L.; Poblet, J.M.; Olmstead, M.M.; Balch, A.L. The Shape of the $Sc_2(\mu_2-S)$ Unit Trapped in C_{82} : Crystallographic, Computational, and Electrochemical Studies of the Isomers, $Sc_2(\mu_2-S)@C_5(6)-C_{82}$ and $Sc_2(\mu_2-S)@C_{30}(8)-C_{82}$. *J. Am. Chem. Soc.* **2011**, *133*, 6752–6760. [[CrossRef](#)]
30. Liu, F.; Wang, S.; Gao, C.-L.; Deng, Q.; Zhu, X.; Kostanyan, A.; Westerström, R.; Jin, F.; Xie, S.-Y.; Popov, A.A.; et al. Mononuclear Clusterfullerene Single-Molecule Magnet Containing Strained Fused-Pentagons Stabilized by a Nearly Linear Metal Cyanide Cluster. *Angew. Chem. Int. Ed.* **2017**, *56*, 1830–1834. [[CrossRef](#)]
31. Yang, S.; Chen, C.; Liu, F.; Xie, Y.; Li, F.; Jiao, M.; Suzuki, M.; Wei, T.; Wang, S.; Chen, Z.; et al. An Improbable Monometallic Cluster Entrapped in a Popular Fullerene Cage: $YCN@C_5(6)-C_{82}$. *Sci. Rep.* **2013**, *3*, 1487. [[CrossRef](#)] [[PubMed](#)]
32. Liu, F.; Gao, C.-L.; Deng, Q.; Zhu, X.; Kostanyan, A.; Westerström, R.; Wang, S.; Tan, Y.-Z.; Tao, J.; Xie, S.-Y.; et al. Triangular Monometallic Cyanide Cluster Entrapped in Carbon Cage with Geometry-Dependent Molecular Magnetism. *J. Am. Chem. Soc.* **2016**, *138*, 14764–14771. [[CrossRef](#)] [[PubMed](#)]
33. Xin, J.; Jin, F.; Guan, R.; Chen, M.; Xie, X.-M.; Zhang, Q.; Xie, S.-Y.; Yang, S. Ancient pigment to treasure: Prussian blue as a cheap solid cyanide/nitrogen dual-source affording the high-yield syntheses of pricey endohedral clusterfullerenes. *Inorg. Chem. Front.* **2021**, *8*, 1719–1726. [[CrossRef](#)]
34. Meng, Q.; Abella, L.; Yang, W.; Yao, Y.-R.; Liu, X.; Zhuang, J.; Li, X.; Echegoyen, L.; Autschbach, J.; Chen, N. $UCN@C_5(6)-C_{82}$: An Encapsulated Triangular UCN Cluster with Ambiguous U Oxidation State [U(III) versus U(I)]. *J. Am. Chem. Soc.* **2021**, *143*, 16226–16234. [[CrossRef](#)] [[PubMed](#)]
35. Shen, W.; Hu, Z.; Yu, P.; Wei, Z.; Jin, P.; Shi, Z.; Lu, X. An experimental and theoretical study of $LuNC@C_{76,82}$ revealing a cage-cluster selection rule. *Inorg. Chem. Front.* **2020**, *7*, 4563–4571. [[CrossRef](#)]
36. Guan, R.; Chen, M.; Xin, J.; Xie, X.-M.; Jin, F.; Zhang, Q.; Xie, S.-Y.; Yang, S. Capturing the Missing Carbon Cage Isomer of C_{84} via Mutual Stabilization of a Triangular Monometallic Cyanide Cluster. *J. Am. Chem. Soc.* **2021**, *143*, 8078–8085. [[CrossRef](#)]

37. Liu, F.; Wang, S.; Guan, J.; Wei, T.; Zeng, M.; Yang, S. Putting a Terbium-Monometallic Cyanide Cluster into the C₈₂ Fullerene Cage: TbCN@C₂(5)-C₈₂. *Inorg. Chem.* **2014**, *53*, 5201–5205. [[CrossRef](#)]
38. Jin, F.; Wang, S.; Yang, S.; Tamm, N.B.; Ioffe, I.N.; Troyanov, S.I. Trifluoromethyl Derivatives of a Monometallic Cyanide Cluster Fullerene, YCN@C₈₂(6)(CF₃)_{16/18}. *Inorg. Chem.* **2016**, *55*, 12523–12526. [[CrossRef](#)]
39. Jin, F.; Wang, S.; Tamm, N.B.; Yang, S.; Troyanov, S.I. Synthesis, Isolation, and Trifluoromethylation of Two Isomers of C₈₄-Based Monometallic Cyanide Clusterfullerenes: Interplay between the Endohedral Cluster and the Exohedral Addends. *Angew. Chem. Int. Ed.* **2017**, *56*, 11990–11994. [[CrossRef](#)]
40. Zuo, T.; Walker, K.; Olmstead, M.M.; Melin, F.; Holloway, B.C.; Echegoyen, L.; Dorn, H.C.; Chaur, M.N.; Chancellor, C.J.; Beavers, C.M.; et al. New egg-shaped fullerenes: Non-isolated pentagon structures of Tm₃N@C_s(51 365)-C₈₄ and Gd₃N@C_s(51 365)-C₈₄. *Chem. Commun.* **2008**, *9*, 1067–1069. [[CrossRef](#)]
41. Krause, M.; Wong, J.; Dunsch, L. Expanding the World of Endohedral Fullerenes—The Tm₃N@C_{2n} (39 ≤ n ≤ 43) Clusterfullerene Family. *Chem. Eur. J.* **2005**, *11*, 706–711. [[CrossRef](#)] [[PubMed](#)]
42. Krause, M.; Liu, X.; Wong, J.; Pichler, T.; Knupfer, M.; Dunsch, L. The Electronic and Vibrational Structure of Endohedral Tm₃N@C₈₀ (I) Fullerene—Proof of an Encaged Tm³⁺. *J. Phys. Chem. A* **2005**, *109*, 7088–7093. [[CrossRef](#)] [[PubMed](#)]
43. Zuo, T.; Olmstead, M.M.; Beavers, C.M.; Balch, A.L.; Wang, G.; Yee, G.T.; Shu, C.; Xu, L.; Elliott, B.; Echegoyen, L.; et al. Preparation and Structural Characterization of the I_h and the D_{5h} Isomers of the Endohedral Fullerenes Tm₃N@C₈₀: Icosahedral C₈₀ Cage Encapsulation of a Trimetallic Nitride Magnetic Cluster with Three Uncoupled Tm³⁺ Ions. *Inorg. Chem.* **2008**, *47*, 5234–5244. [[CrossRef](#)]
44. Che, Y.; Yang, H.; Wang, Z.; Jin, H.; Liu, Z.; Lu, C.; Zuo, T.; Dorn, H.C.; Beavers, C.M.; Olmstead, M.M.; et al. Isolation and Structural Characterization of Two Very Large, and Largely Empty, Endohedral Fullerenes: Tm@C_{3v}-C₉₄ and Ca@C_{3v}-C₉₄. *Inorg. Chem.* **2009**, *48*, 6004–6010. [[CrossRef](#)] [[PubMed](#)]
45. Wang, Z.; Izumi, N.; Nakanishi, Y.; Koyama, T.; Sugai, T.; Tange, M.; Okazaki, T.; Shinohara, H. Near-Infrared Photoluminescence Properties of Endohedral Mono- and Dithulium Metallofullerenes. *ACS Nano* **2016**, *10*, 4282–4287. [[CrossRef](#)] [[PubMed](#)]
46. Krätschmer, W.; Lamb, L.D.; Fostiropoulos, K.; Huffman, D.R. Solid C₆₀: A new form of carbon. *Nature* **1990**, *347*, 354–358. [[CrossRef](#)]
47. Xu, Y.-Y.; Tian, H.-R.; Li, S.-H.; Chen, Z.-C.; Yao, Y.-R.; Wang, S.-S.; Zhang, X.; Zhu, Z.-Z.; Deng, S.-L.; Zhang, Q.; et al. Flexible decapyrrolicorannulene hosts. *Nat. Commun.* **2019**, *10*, 485. [[CrossRef](#)]
48. Yao, Y.-R.; Roselló, Y.; Ma, L.; Puente Santiago, A.R.; Metta-Magaña, A.; Chen, N.; Rodríguez-Forteza, A.; Poblet, J.M.; Echegoyen, L. Crystallographic Characterization of U@C_{2n} (2n = 82–86): Insights about Metal-Cage Interactions for Mono-metallofullerenes. *J. Am. Chem. Soc.* **2021**, *143*, 15309–15318. [[CrossRef](#)]
49. Sabirov, D.S.; Ori, O.; László, I. Isomers of the C₈₄ fullerene: A theoretical consideration within energetic, structural, and topological approaches. *Fuller. Nanotub. Car. N.* **2018**, *26*, 100–110. [[CrossRef](#)]
50. Kirbach, U.; Dunsch, L. The Existence of Stable Tm@C₈₂ Isomers. *Angew. Chem. Int. Ed.* **1996**, *35*, 2380–2383. [[CrossRef](#)]
51. Sado, Y.; Aoyagi, S.; Kitaura, R.; Miyata, Y.; Nishibori, E.; Sawa, H.; Sugimoto, K.; Shinohara, H. Structure of Tm@C₈₂(I) Metallofullerene by Single-Crystal X-ray Diffraction Using the 1:2 Co-Crystal with Octaethylporphyrin Nickel (Ni(OEP)). *J. Phys. Chem. C* **2013**, *117*, 6437–6442. [[CrossRef](#)]
52. Kodama, T.; Ozawa, N.; Miyake, Y.; Sakaguchi, K.; Nishikawa, H.; Ikemoto, I.; Kikuchi, K.; Achiba, Y. Structural Study of Three Isomers of Tm@C₈₂ by ¹³C NMR Spectroscopy. *J. Am. Chem. Soc.* **2002**, *124*, 1452–1455. [[CrossRef](#)] [[PubMed](#)]
53. Pichler, T.; Golden, M.S.; Knupfer, M.; Fink, J.; Kirbach, U.; Kuran, P.; Dunsch, L. Monometallofullerene Tm@C₈₂: Proof of an Encapsulated Divalent Tm Ion by High-Energy Spectroscopy. *Phys. Rev. Lett.* **1997**, *79*, 3026–3029. [[CrossRef](#)]
54. Pichler, T.; Knupfer, M.; Golden, M.S.; Böske, T.; Fink, J.; Kirbach, U.; Kuran, P.; Dunsch, L.; Jung, C. The metallofullerene Tm@C₈₂: Isomer-selective electronic structure. *Appl. Phys. A* **1998**, *66*, 281–285. [[CrossRef](#)]
55. Lu, X.; Slanina, Z.; Akasaka, T.; Tsuchiya, T.; Mizorogi, N.; Nagase, S. Yb@C_{2n} (n = 40, 41, 42): New Fullerene Allotropes with Unexplored Electrochemical Properties. *J. Am. Chem. Soc.* **2010**, *132*, 5896–5905. [[CrossRef](#)]
56. Bao, L.; Pan, C.; Slanina, Z.; Uhlik, F.; Akasaka, T.; Lu, X. Isolation and Crystallographic Characterization of the Labile Isomer of Y@C₈₂ Cocrystallized with Ni(OEP): Unprecedented Dimerization of Pristine Metallofullerenes. *Angew. Chem. Int. Ed.* **2016**, *55*, 9234–9238. [[CrossRef](#)]
57. Kikuchi, K.; Nakao, Y.; Suzuki, S.; Achiba, Y.; Suzuki, T.; Maruyama, Y. Characterization of the Isolated Y@C₈₂. *J. Am. Chem. Soc.* **1994**, *116*, 9367–9368. [[CrossRef](#)]
58. Suzuki, T.; Maruyama, Y.; Kato, T.; Kikuchi, K.; Achiba, Y. Electrochemical properties of La@C₈₂. *J. Am. Chem. Soc.* **1993**, *115*, 11006–11007. [[CrossRef](#)]
59. Akasaka, T.; Okubo, S.; Kondo, M.; Maeda, Y.; Wakahara, T.; Kato, T.; Suzuki, T.; Yamamoto, K.; Kobayashi, K.; Nagase, S. Isolation and characterization of two Pr@C₈₂ isomers. *Chem. Phys. Lett.* **2000**, *319*, 153–156. [[CrossRef](#)]
60. Hu, S.; Liu, T.; Shen, W.; Slanina, Z.; Akasaka, T.; Xie, Y.; Uhlik, F.; Huang, W.; Lu, X. Isolation and Structural Characterization of Er@C_{2v}(9)-C₈₂ and Er@C_s(6)-C₈₂: Regioselective Dimerization of a Pristine Endohedral Metallofullerene Induced by Cage Symmetry. *Inorg. Chem.* **2019**, *58*, 2177–2182. [[CrossRef](#)]
61. Cai, W.; Morales-Martínez, R.; Zhang, X.; Najera, D.; Romero, E.L.; Metta-Magaña, A.; Rodríguez-Forteza, A.; Fortier, S.; Chen, N.; Poblet, J.M.; et al. Single crystal structures and theoretical calculations of uranium endohedral metallofullerenes (U@C_{2n}, 2n = 74, 82) show cage isomer dependent oxidation states for U. *Chem. Sci.* **2017**, *8*, 5282–5290. [[CrossRef](#)]

62. Liu, X.; Zuo, T.; Dorn, H.C. Polarizability Effects Dominate the Chromatographic Retention Behavior of Spheroidal and Elipsoidal Metallofullerene Nanospheres. *J. Phys. Chem. C* **2017**, *121*, 4045–4049. [[CrossRef](#)]
63. Liu, X.; Dorn, H.C. DFT prediction of chromatographic retention behavior for a trimetallic nitride metallofullerene series. *Inorg. Chim. Acta* **2017**, *468*, 316–320. [[CrossRef](#)]
64. Dolomanov, O.V.; Bourhis, L.J.; Gildea, R.J.; Howard, J.A.K.; Puschmann, H. OLEX2: A complete structure solution, refinement and analysis program. *J. Appl. Cryst.* **2009**, *42*, 339–341. [[CrossRef](#)]
65. Sheldrick, G. Crystal structure refinement with SHELXL. *Acta Crystallogr. Sect. C* **2015**, *71*, 3–8. [[CrossRef](#)] [[PubMed](#)]
66. Spek, A. PLATON SQUEEZE: A tool for the calculation of the disordered solvent contribution to the calculated structure factors. *Acta Crystallogr. Sect. C* **2015**, *71*, 9–18. [[CrossRef](#)]

Disclaimer/Publisher's Note: The statements, opinions and data contained in all publications are solely those of the individual author(s) and contributor(s) and not of MDPI and/or the editor(s). MDPI and/or the editor(s) disclaim responsibility for any injury to people or property resulting from any ideas, methods, instructions or products referred to in the content.